Science of the Total Environment 650 (2019) 1832–1845

Contents lists available at ScienceDirect

Science of the Total Environment

journal homepage: www.elsevier.com/locate/scitotenv

Factors controlling sediment and nutrient fluxes in a small microtidal salt marsh within the Venice Lagoon

Bonometto A. *, Feola A., Rampazzo F., Gion C., Berto D., Ponis E., Boscolo Brusà R.

Italian National Institute for Environmental Protection and Research, ISPRA, Loc. Brondolo, 30015 Chioggia, Venezia, Italy

HIGHLIGHTS

- Sediment and nutrients fluxes within saltmarshes were studied.
- Fluxes were assessed by coupling field sampling and HD modeling.
- The saltmarsh resulted to act alternatively as a sink or as a source.
- Sediment and nutrient concentrations during flow phase and tidal excursion resulted the most important controlling factors.
- Vegetated intertidal area provided the major nitrogen removal function.

GRAPHICAL ABSTRACT

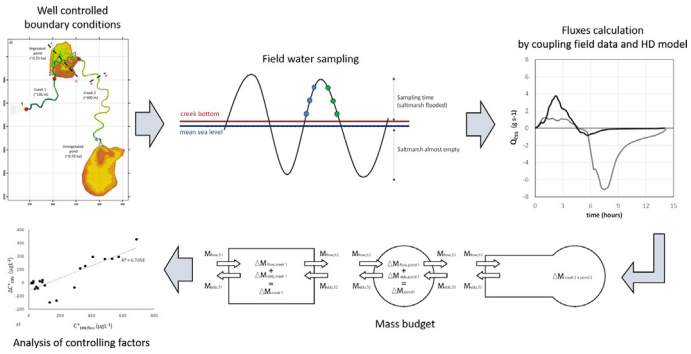

ARTICLE INFO

Article history:
Received 16 February 2018
Received in revised form 7 September 2018
Accepted 10 September 2018
Available online 12 September 2018

Keywords:
Nutrient fluxes
Sediment fluxes
Salt marshes
Lagoon

ABSTRACT

Coastal salt marshes are among the Earth's most productive ecosystems and provide a number of ecosystem services. Water quality regulation by storing, transforming and releasing nutrients, organic matter and suspended sediment is recognized as one of the most important functions of salt marshes. The self-purification capacity of intertidal ecosystems contributes to mitigating nutrient inputs, acting as a buffer zone between watersheds and coastal waters, especially in relation to climate change and the increasing frequency of impulsive extreme events. Understanding sediment and nutrient fluxes and assessing the mechanisms that control them are valuable for the preservation and future restoration of salt marshes and for enhancing their effectiveness in providing water quality regulation services.

To investigate the main driving factors in microtidal environments, changes in suspended sediment and nutrient concentrations were measured during several tidal cycles in a small microtidal reconstructed salt marsh in the Venice Lagoon, which was selected as the experimental site. The tidal amplitude, nutrients and total suspended solid concentrations were measured during 6 tidal cycles between September 2011 and October 2013. The water discharge was derived by forcing the hydrodynamic MIKE-DHI numerical model with the measured tidal levels. Fluxes were assessed by coupling field data with the calculated discharges. The salt marsh filtering function was related to the inflow matter concentrations and tidal amplitude. When high suspended solid and nutrient concentrations enter the salt marsh, accumulation processes prevail on release. In contrast, in the case of low concentrations and high tidal excursion, the salt marsh functions as a nutrient and sediment source. During all campaigns, the nitrogen removal function was more effective within the intertidal vegetated areas. Sediment release was the dominant process in the outermost creek, whereas sedimentation prevailed in the inner area of the salt marsh because of the attenuation of hydrodynamic forcing during tide propagation.

* Corresponding author.
E-mail address: andrea.bonometto@isprambiente.it (A. Bonometto).

https://doi.org/10.1016/j.scitotenv.2018.09.142
0048-9697/

1. Introduction

Salt marshes are highly productive ecosystems and are widely distributed, globally covering 200,000–400,000 km^2 (Fagherazzi et al., 2013). These intertidal habitats provide distinctive biodiversity and other important ecosystem services, including coastal protection, carbon sequestration, fishery support, nutrient cycling and water quality regulation (Mossman et al., 2012; Temmerman et al., 2013; Costanza et al., 1997).

Understanding the role that tidal salt marshes play in nutrient and sediment dynamics is an open issue in the fields of research focused on transitional waters (i.e., estuaries, lagoons, brackish wetlands and similar). Studies regarding nutrients and organic matter tidal fluxes between salt marshes and adjacent waters receive significant attention from scientists and managers because of their influence on both water quality and availability of essential elements at the base of the food web (Piehler and Smyth, 2011). Several authors have investigated the nutrient removal function of salt marshes, concluding that salt marshes act as a sink of nutrients and organic matter (Etheridge et al., 2014; Velinsky et al., 2017; Poulin et al., 2009); it has also been emphasized that vegetated and structured habitats enhance the efficiency of denitrification processes (Piehler and Smyth, 2011).

The purification capacity of intertidal ecosystems could play an important role in the mitigation of nutrient inputs, acting as a buffer zone between watersheds and coastal waters, especially in relation to climate change and the increase in impulsive extreme events (Etheridge et al., 2014). However, other studies obtained opposite results, following the so-called "Outwelling Hypothesis" (Dame et al., 1986; Odum, 1980), postulating that salt marshes are exporters of organic matter to the coastal zone, providing food resources that support marine productivity in coastal systems (Simas and Ferreira, 2007; Whiting et al., 1985).

Quantification of sediment fluxes in coastal tidal marshes is a widespread theme throughout the literature, mainly related to examination of deposition-erosion rates and morphological evolution (Ganju et al., 2005). Sediment transport within salt marsh systems is driven by tidal and storm forcing, external sediment input, internal sediment redistribution and trapping of sediment by marsh vegetation (Rosencranz et al., 2016). The import-export of suspended sediment plays an important role in the formation and maintenance of tidal salt marshes (Rosencranz et al., 2016; Ganju et al., 2005; Reed et al., 1999; Fagherazzi et al., 2013). Sediment deposition, along with accumulation of autochthonous organic material, contributes to the vertical accretion, increasing the resilience of salt marshes to sea level rises (Reed, 1989; Morris et al., 2002; Mudd et al., 2009). Thus, healthy salt marshes are net sediment sinks (Fagherazzi et al., 2013). Conversely, if the sediment release rate is greater than the deposition rate, the salt marsh will enter into an erosive state, which can be potentially irreversible even in the absence of sea level rises (Mariotti and Fagherazzi, 2013).

Due to the value of these ecosystems, many regulatory agencies seek to protect existing tidal marshes and restore lost ones (Ganju et al., 2005, 2017). In his policy paper, originally produced in response to a request from the Scientific and Technical Review Panel of the Ramsar Convention on Wetlands, Erwin (2009) remarked that policymakers should promote wetland restoration as part of their climate change adaptation and mitigation strategies.

Understanding the factors controlling sediment and nutrient fluxes within salt marshes is an essential goal to make effective decisions about salt marsh management and restoration (Reed et al., 1999; Erwin, 2009). Assessments of sediment dynamics within salt marshes, even on short (i.e., tidal) time scales, might be useful for long-term resource management, especially in relation to sea level rises. Moreover, understanding nutrient dynamics would support the design of restoration projects aimed at enhancing the provision of targeted ecosystem services.

Most studies regarding nutrient and sediment fluxes between salt marshes and adjacent waters have been performed in ocean estuarine ecosystems, whereas only limited information about microtidal Mediterranean lagoons is available in the literature. The purpose of this paper is to contribute to understanding the dynamics in Mediterranean microtidal lagoons.

A small reconstructed salt marsh was selected as the study site to investigate the factors controlling sediment and nutrient fluxes. The site has well-controlled boundary conditions that are ensured by the elevation of creek and pond edges, which also prevent lateral water flow during high tide.

2. Material and methods

2.1. Study site

The study site is located in Italy, in the southern part of the Venice Lagoon, close to the city of Chioggia (Fig. 1a). It is part of an artificially constructed salt marsh made in 1992 by *Magistrato alle Acque di Venezia* (Venice Water Authority). A system of creeks and ponds was dredged 4 years after the salt marsh construction with a renaturalization purpose (Fig. 1b). The dredged material was placed along the edges of creeks and ponds, which resulted in them being completely embanked (Fig. 1c). The banks are topped only by exceptionally high tides, a few times per year. Consequently, the flow and ebb tides enter the system only from the mouth of creek 1, and lateral fluxes are prevented during tidal propagation through the salt marsh. The present study focuses on the resulting hydraulic system, which includes two ponds and two creeks connected with the adjacent tidal flat by a single channel mouth (Fig. 1d).

Within the first vegetated pond, during low tide, the tidal flow remains channeled, whereas during higher tide levels, the water floods the intertidal vegetated platform (Fig. 1c). Because of the bottom elevation, only the first pond is vegetated (*Salicornia*, *Puccinellia* and *Sarcocornia* spp.). The second pond, in the terminal part of the system (Fig. 1d), is often covered by a thin layer of water due to tidal time delay and amplitude attenuation.

Given its structural features, this system is an excellent experimental site, with easily controllable and measurable boundary conditions.

Previous studies have addressed changes in the morphological features of this site through remote sensing, field surveys and mathematical modeling (D'Alpaos et al., 2007; Guarnieri et al., 2009).

2.2. Sampling design

Water sampling was performed during six semidiurnal tidal cycles from September 2011 to October 2013 in different seasons (I: 28/09/2011; II: 09/03/2012; III: 26/06/2012; IV: 08/05/2013; V: 23/07/2013; VI: 17/10/2013). Organic matter, dissolved organic carbon (DOC), particulate organic carbon (POC), nutrient concentrations (ammonia NH_4^+, nitrate NO_3^-, nitrite NO_2^-, and orthophosphate PO_4^-) and total suspended solids (TSS) were measured during the flow and ebb tide. For each tidal phase, samples were collected following a water-level-based approach, sampling at intervals of approximately 0.15 m of water depth variation. Therefore, the sampling frequency ranged from 30′ to 90′, depending on the tidal gradient. During each campaign, the first sample was taken when water began to flow into the salt marsh and at all stations, the water depth was at least 10 cm, being the minimum level needed for collecting samples by bottle. Similarly, the final sample was collected during the ebb phase before the water depth decreased below 10 cm. Usually, at the end of the ebb phase, the salt marsh was almost completely empty.

These four stations were selected as representative of fluxes between the salt marsh and adjacent waters and the dynamics within the intertidal system. In particular, at Station 1, located at the mouth of the first creek, changes in water quality are expected to be a result

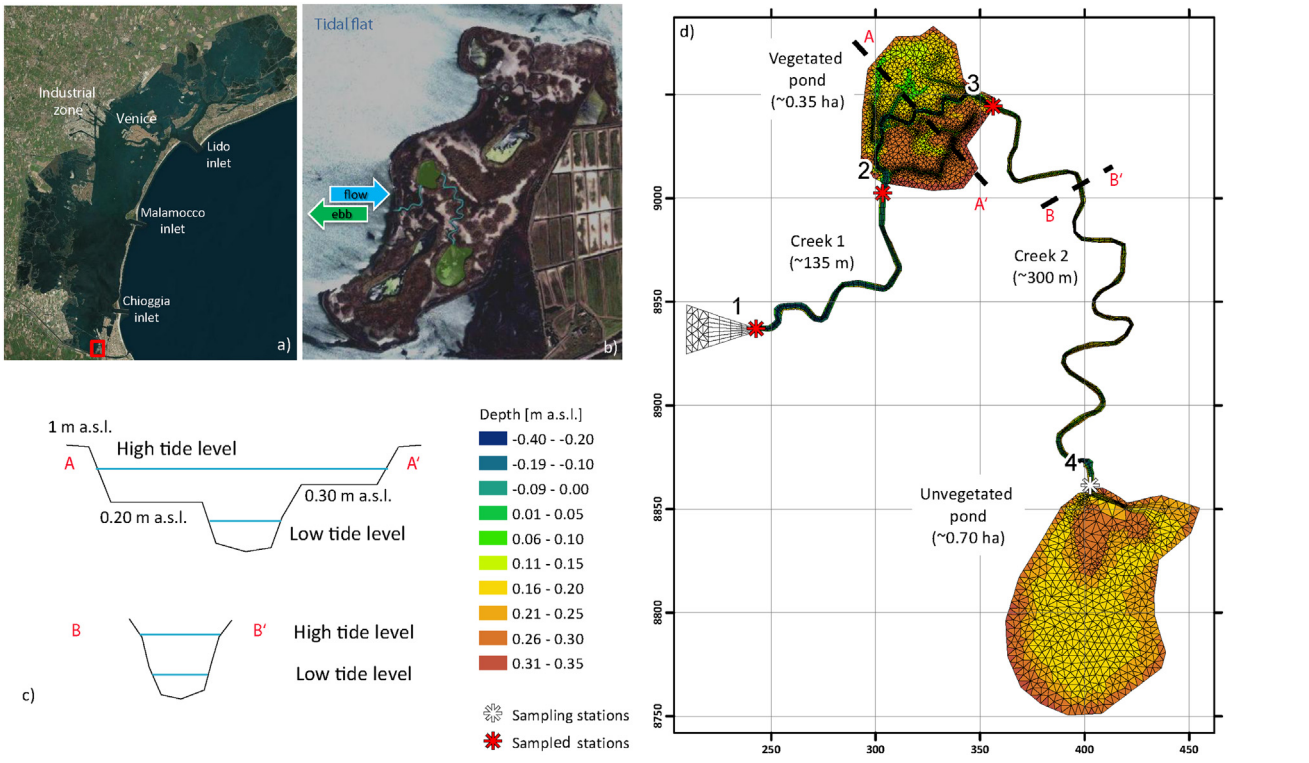

Fig. 1. The site area is located in the south of the Venice Lagoon (a), within a constructed salt marsh (b). The system of two creeks and two ponds is completely embanked (c). The flow and ebb tides enter the system from a single channel section (cross section 1). All monitoring stations and corresponding cross sections (asterisks) are reported (d). Because of bathymetry and different water drainage by small tidal creeks, only one of the two ponds is vegetated.

of all the processes occurring within the study site during each tidal cycle. Cross sections 2, 3 and 4 were placed at the beginning and at the end of each morphological element (first and second creek, vegetated and unvegetated ponds). Station 4 was added in May 2013 (campaign IV) to assess the dynamics within the inner unvegetated pond.

All campaigns were performed during spring tides, when the higher parts of the vegetated pond were also flooded. Moreover, during spring tides, there was a sufficient amount of water in the system to allow sufficient time to complete multiple measurements.

2.3. Water sampling

Sampling and laboratory activities were performed according to the methods described in Sfriso et al. (2014). Water samples were analyzed for NH_4^+, NO_2^- and NO_3^- DOC, POC and TSS. Temperature, salinity, dissolved oxygen (DO), phytoplankton chlorophyll-*a* (Chl-*a*), orthophosphate (PO_4^-) and total particulate nitrogen (TPN) were also determined (but not discussed in this paper).

Three replicates of the whole water column were collected for each sample. Water subsamples were filtered via Whatman GF/F filters (porosity 0.7 μm) for TSS determination and cellulose acetate Sartorius filters for laboratory nutrient determination.

DOC concentrations of seawater samples were measured with a Shimadzu TOC VCPN Analyzer using a silica catalyst. Potassium hydrogen phthalate was used as standard. The reproducibility of the analytical procedure was within 2–3%.

POC was determined with a CHN Elemental Analyzer Thermo Fisher Scientific Flash 2000 (Thermo Fisher Scientific, Bremen, Germany), after acidification with HCl (1 N), to remove the inorganic carbonate fraction. Acetanilide was used as standard. The reproducibility of the analytical system was <2%. Nutrient analyses were performed with an automatic multichannel analyzer Seal Quaattro (SEAL analytical Ltd., West Sussex, UK) using spectrophotometrical methods according to Strickland and Parsons (1984).

2.4. Water flux assessment

The description of local hydrodynamics and water fluxes through the cross sections at the sampling sites were calculated by implementing the numerical model DHI-MIKE for the study site. The MIKE Hydrodynamic module (HD) solves the momentum equations and continuity equation, simulating the water level variation and current velocities with respect to a variety of forcing functions (tidal elevations and wind) and local bathymetry (Moharir et al., 2014). A flexible mesh was designed; the mesh combined triangular and rectangular elements (Fig. 1d), to properly describe the pond surface and creeks, respectively. A brief description of the mesh, input data and model calibration is reported in Appendix A.

Intertidal topography and creek bathymetry were taken from previous studies (Venice Water Authority, unpublished data; Guarnieri et al., 2009). Additional data were collected with a specific campaign (Trimble Geo 7X instrument) for digital terrain model optimization. Boundary conditions of tidal level and wind forcing were collected from a nearby station (Chioggia-Vigo), part of the meteo-mareographic network of ISPRA (www.venezia.isprambiente.it/meteo-mareographic-network).

Measurements of water level were collected during each campaign's tidal cycle at all 4 sampling stations to calibrate the hydrodynamic model.

2.5. Calculation of sediment and nutrient fluxes

In this salt marsh, selected as the study site, all suspended sediments and nutrients, transported by tidal flow, enter through the first creek mouth (cross section S1) (Fig. 1).

Following Etheridge et al. (2014) and Fagherazzi et al. (2013), a mass balance approach (i.e., the difference between the inflow and outflow budget) was used to determine whether the constructed tidal marsh system acts as a sink or as a source of suspended sediments and

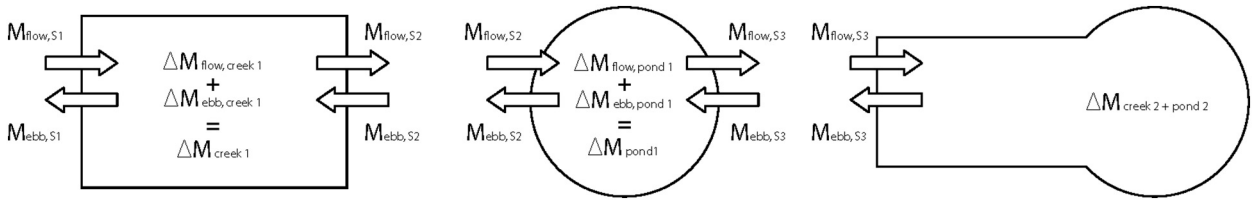

Fig. 2. Sketch of the entire system, divided into morphological elements (creek 1, pond 1, creek 2 and pond 2), and specification of flow and ebb mass fluxes at each cross section (S1, S2, S3). The mass balance (ΔM_E), evaluated using Eq. (3), is indicated for each morphological element (E).

nutrients over the different tidal phases. The whole system was evaluated as a series of morphological elements (E), each of which was defined by cross sections (S) (Fig. 2).

The inflowing mass ($M_{flow,S}$) entering the study site at each cross section (S) during the incoming tide was calculated using the following equation:

$$M_{flow,S} = \sum_{flow} q_i c_i \Delta t \quad (1)$$

where q_i is the water discharge ($m^3\ s^{-1}$), c_i is the concentration (μg, mg L^{-1}) at time i, and Δt is the time interval (10 min). The term $q_i c_i$ represents the mass flow rate ($Q_{DIN,S}$, mg s^{-1}; $Q_{TOC,S}$, g s^{-1}, $Q_{TSS,S}$, g s^{-1}) at station S and time i.

Since the water samples were collected with a frequency ranging from 30 to 90 min (see Section 2.2), the measured concentration data were transformed into 10-min data via linear interpolation.

The same equation was applied to assess the outflowing mass during the ebb ($M_{ebb,S}$).

Differences between $M_{flow,S}$ and $M_{ebb,S}$ provide the net mass balance (ΔM_S, Fig. 2) at each cross section (S) and are calculated as

$$\Delta M_S = M_{flow,S} - M_{ebb,S} \quad (2)$$

Differences between mass fluxes at two consecutive cross sections were calculated to estimate the accumulation-release dynamics within different morphological elements (E) (e.g., creek 1, pond 1, etc.; Fig. 2) during flow and ebb ($\Delta M_{flow,E}$; $\Delta M_{ebb,E}$).

Taking as an example the morphological element creek 1, delimited by cross sections S1 and S2, the mass budget for the element is calculated as

$$\Delta M_E = \Delta M_{flow,E} + \Delta M_{ebb,E} \quad (3)$$

where

$$\Delta M_{flow,E} = (M_{flow,S1} - M_{flow,S2})$$

$$\Delta M_{ebb,E} = (M_{ebb,S2} - M_{ebb,S1}) \quad (3b)$$

Positive and negative values of ΔM_E indicate, respectively, matter accumulation and release within the element.

In Fig. 2, a sketch of the entire system, divided into morphological elements (creek 1, pond 1, creek 2 and pond 2), is presented. The flow and ebb mass fluxes are specified at each cross section (S1, S2, S3). The mass balance (ΔM_E), evaluated using Eq. (3), is indicated for each morphological element (E).

Since station 4 was monitored only during the last 3 campaigns; to provide homogeneous analysis, data from station 4 were not used in the net mass budget calculation. Therefore, ΔM_{S3} is equal to the net budget for creek 2 and pond 2 evaluated as a whole (Fig. 2).

2.6. Volume-weighted mean concentration

Statistical analysis was performed using the computing environment R (R Development Core Team, 2005) to investigate the factors controlling sediment and nutrient dynamics. Changes in the *volume-weighted mean* concentrations (c*) between flowing and ebbing water were related to the input concentration and tidal height for each sample date.

The volume-weighted mean concentrations (c*) for each campaign were determined at each station (ST) using the following equation:

$$c * ST = \frac{\sum_{flow,} q_i c_i}{\sum_{flow} q_i} \quad (4)$$

where q_i and c_i have already been defined in 1.5. As suggested in previous studies (Daly and Mathieson, 1981; Heinle and Flemer, 1976), the volume-weighted mean prevents errors in the assessment of accumulation and release processes due to differences in water volume

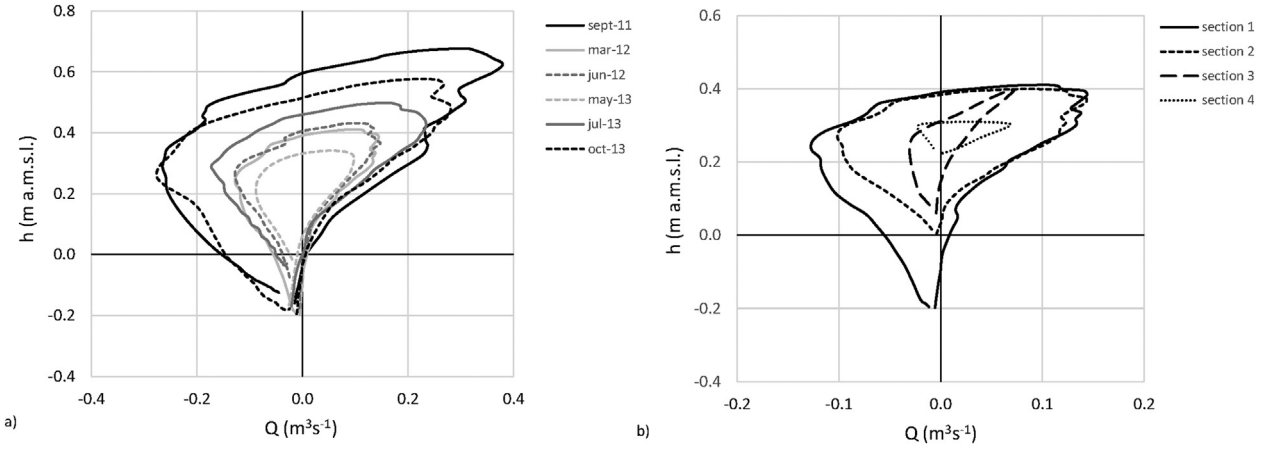

Fig. 3. a) Stage-flow curves at station 1 for each sampling date. b) Stage-flow curves at stations 1, 2, 3, and 4 for the II campaign's tidal cycle (March 9th, 2013).

Table 1
Calculated data for the total mass (M_{DIN}, M_{TSS}, M_{DOC}, M_{POC}) entering and exiting the system during flow and ebb tide through section 1 for each campaign. The volume of water exchanged during flow and ebb is also reported (VOL). The cross section 1 is representative of global fluxes between salt marsh and adjacent waters. Positive values of ΔM (sink) are highlighted in blue, whereas negative values (source) are highlighted in red.

Campaign	Data	Cross section	$M_{DIN,flow}$	$M_{DIN,ebb}$	ΔM_{DIN}	$M_{TSS,flow}$	$M_{TSS,ebb}$	ΔM_{TSS}	$M_{DOC,flow}$	$M_{DOC,ebb}$	ΔM_{DOC}	$M_{POC,flow}$	$M_{POC,ebb}$	ΔM_{POC}	VOL_{flow} (m^3)	VOL_{ebb} ($m^3 10^3$)	ΔVOL ($m^3 10^3$)
			(g)			(kg)			(kg)			(kg)			($m^3 10^3$)		
I	28/09/2011	1	148	297	−149	13.9	86.8	−72.9	26.1	18.0	8.1	2.3	4.5	−2.3	3.81	−3.53	0.28
II	09/03/2012	1	461	279	182	27.8	7.1	20.7	3.1	4.0	−0.9	0.7	0.4	0.3	1.28	−1.19	0.09
III	26/06/2012	1	76	120	−43	8.3	5.9	2.3	7.1	8.4	−1.3	1.2	1.0	0.2	1.61	−1.53	0.08
IV	08/05/2013	1	69	97	−28	4.5	5.0	−0.5	6.6	5.5	1.1	0.8	0.9	−0.1	0.68	−0.8	−0.12
V	23/07/2013	1	54	29	26	30.6	15.8	14.7	13.0	13.7	−0.7	8.7	6.6	2.0	1.9	−1.76	0.14
VI	17/10/2013	1	1755	943	812	10.3	10.7	−0.4	9.8	9.6	0.2	2.8	2.4	0.3	3.06	−2.49	0.57

exchanged during flow and ebb. For example, when the volume of water entering the system during a flood tide is greater than the volume flowing out of the system during the ebb tide, an amount of dissolved and particulate matter would be stored within the system, even if no deposition or removal processes actually occurred, and vice versa.

3. Results and discussion

3.1. Tidal excursion and water fluxes

Although all campaigns were performed during spring tides (see Section 2.2), the tidal amplitude and exchanged water volume strongly differed between dates (Table B.1). The tidal peaks ranged between +0.68 m a.m.s.l. on September 28th, 2011 and +0.37 m a.m.s.l. on May 8th, 2013. The tidal amplitude was approximately 20% lower at the inner site (ST.4) than at the creek mouth (ST.1) due to attenuation along the salt marsh.

The volume that flowed into the study site during each tidal cycle ranged between 3.81×10^3 m^3 on September 28th, 2011 and 0.68×10^3 m^3 on May 8th, 2013.

The stage-flow curves at station 1 were examined using simulated data from a numerical model (see Section 2.4). Stage-flow curves provide an integrated description of hydrodynamic, including tidal peak height, tidal excursion and water discharge (Fig. 3a). The values of these hydrodynamic parameters (Table B.1) were highest for campaign I (Sep. 11) and lowest for IV (May 13). Furthermore, the values of the hydrodynamic parameters decrease progressively upon entering the salt marsh system (Fig. 3b), from creek 1 (ST.1) to the inner pond (ST.4).

Previous studies (Marani et al., 2003; Fagherazzi et al., 2013 and reference therein) have discussed the asymmetry of stage-flow curves, highlighting the occurrence of maximum discharge during the flood and ebb tides. As also observed by Etheridge et al. (2015), it did not always occur at the point where water begins to spread over the marsh platform on the flooding tide (bankfull stage; at this study site, +0.30 m a.m.s.l. – see Section 2.1). Indeed, in the tidal cycles characterized by the highest peaks (campaign I and VI), the maximum discharge occurred when the water level was 0.5–0.6 m a.m.s.l., which is 0.20–0.30 m above the bankfull stage (Fig. 2a). No deviation from the behavior described by Fagherazzi et al. (2013) was observed during the ebb phase, as the maximum ebb flow rate occurred when water level was below the bank-full stage.

3.2. Sediment and nutrient fluxes

The fluxes entering and exiting the system through the cross section 1, placed at the boundary between the salt marsh system and the adjacent tidal flat (Fig. 1), were assessed to determine the total mass budget of nitrogen (DIN) and suspended sediment (TSS). In Fig. B.1, an example flux calculation based on measured and interpolated data coupled with hydrodynamic modeling is reported for the March 9th, 2012 campaign. The nutrient and suspended sediment fluxes at the tidal scale revealed different dynamics. The direction and magnitude of fluxes between the salt marsh system and adjacent waters were found to be highly variable: the system acted alternately as a sink and source of matter (Table 1). In Fig. 4, the fluxes of DIN and TSS through section 1 are reported.

A major export dynamic was observed during campaign I; $M_{DIN,flow,S1} = 148$ g entered the salt marsh through creek 1 mouth

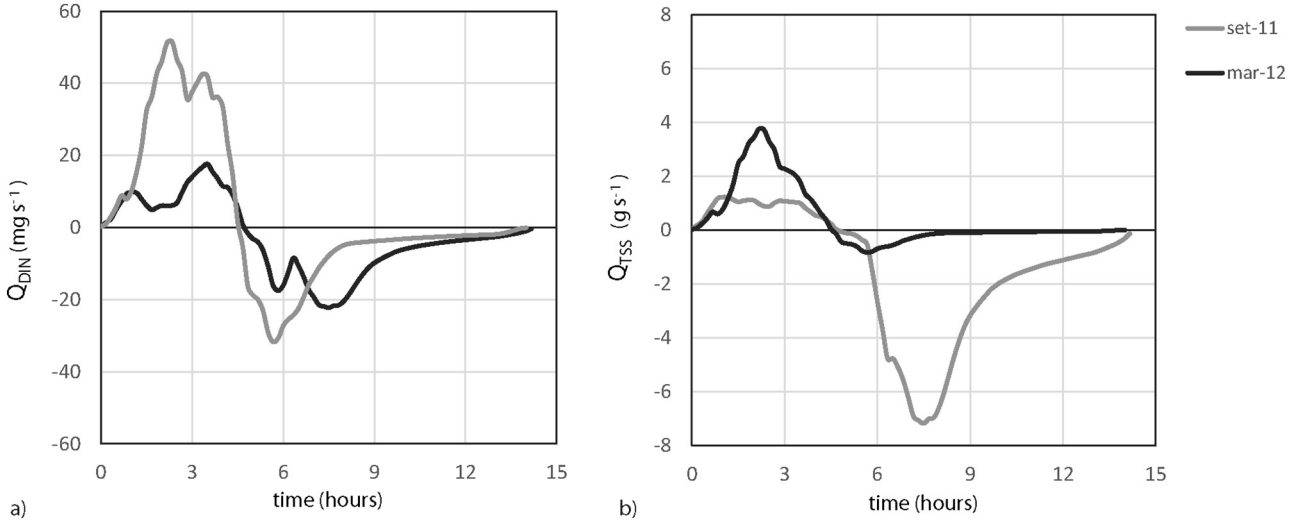

Fig. 4. a) Fluxes of DIN (mg s^{-1}) and TSS (g s^{-1}) crossing section 1 on September 28th, 2011 (gray line) and March 9th, 2012 (black line). The areas under the curves represents the total mass entering in the system during flow tide ($M_{TSS,flow}$; $M_{DIN,flow}$) and exiting the system during ebb tide ($M_{TSS,ebb}$; $M_{DIN,ebb}$, negative values).

Table 2
Volume-weighted mean water concentration (see Section 2.6, Eq. (4)) of DIN, TSS, DOC and POC in flow (C^*_{flow}) and ebb (C^*_{ebb}) tides. Changes in the volume-weighted mean concentration are also reported as $\Delta C^* = C^*_{flow} - C^*_{ebb}$.

Campaign	Data	Cross section	$C^*_{DOC,flow}$ mg L^{-1}	$C^*_{DOC,ebb}$ mg L^{-1}	ΔC^*_{DOC} mg L^{-1}	$C^*_{POC,flow}$ mg L^{-1}	$C^*_{POC,ebb}$ mg L^{-1}	ΔC^*_{POC} mg L^{-1}	$C^*_{DIN,flow}$ μg L^{-1}	$C^*_{DIN,ebb}$ μg L^{-1}	ΔC^*_{DIN} μg L^{-1}	$C^*_{TSS,flow}$ mg L^{-1}	$C^*_{TSS,ebb}$ mg L^{-1}	ΔC^*_{TSS} mg L^{-1}
I	28/09/2011	2	6.9	5.1	1.8	0.6	1.3	−0.7	39.0	84.1	−45.1	3.7	24.6	−20.9
I	28/09/2011	3	5.7	6.4	−0.7	0.8	1.1	−0.3	69.9	57.3	12.6	8.9	16.5	−7.6
I	28/09/2011	4	4.9	6.3	−1.5	0.7	0.8	−0.1	57.5	100.0	−42.5	7.8	4.4	3.4
II	09/03/2012	2	2.5	3.3	−0.9	0.5	0.3	0.2	360.1	233.4	126.7	21.7	6.0	15.8
II	09/03/2012	3	3.1	3.4	−0.3	0.5	0.3	0.2	408.5	212.3	196.1	15.7	6.1	9.6
II	09/03/2012	4	2.9	3.3	−0.4	0.4	0.5	−0.1	328.1	219.8	108.4	10.0	10.2	−0.1
III	26/06/2012	2	4.4	5.5	−1.0	0.8	0.7	0.1	47.5	78.3	−30.8	5.1	3.9	1.3
III	26/06/2012	3	5.3	6.4	−1.1	0.7	0.3	0.4	87.3	67.2	20.1	4.6	4.1	0.4
III	26/06/2012	4	5.0	5.4	−0.4	0.7	0.6	0.1	85.2	80.8	4.4	4.9	2.2	2.7
IV	08/05/2013	2	9.8	6.8	2.9	1.2	1.1	0.1	101.4	120.3	−18.8	6.7	6.2	0.5
IV	08/05/2013	3	8.8	7.3	1.5	1.4	0.9	0.5	133.0	281.4	−148.4	8.2	5.4	2.8
IV	08/05/2013	4	8.1	8.2	−0.1	1.2	1.0	0.2	176.7	311.1	−134.4	6.3	4.4	1.9
IV	08/05/2013	5	8.7	9.8	−1.1	1.3	4.0	−2.6	291.0	327.2	−36.2	8.2	16.4	−8.3
V	23/07/2013	2	6.8	7.8	−1.0	4.6	3.8	0.8	28.6	16.3	12.3	16.1	9.0	7.1
V	23/07/2013	3	7.2	7.2	0.0	6.3	3.2	3.1	17.4	18.5	−1.1	19.3	8.8	10.5
V	23/07/2013	4	8.0	7.3	0.7	4.5	4.1	0.4	16.1	18.7	−2.6	14.8	11.2	3.5
V	23/07/2013	5	9.3	7.6	1.7	3.6	4.4	−0.8	27.1	28.5	−1.4	9.4	13.1	−3.7
VI	17/10/2013	2	3.2	3.8	−0.7	0.9	1.0	−0.1	573.7	378.3	195.4	3.4	4.3	−0.9
VI	17/10/2013	3	3.7	4.2	−0.4	1.1	0.9	0.2	531.6	349.9	181.6	6.3	4.8	1.6
VI	17/10/2013	4	4.3	4.0	0.3	1.2	0.8	0.4	485.9	307.1	178.8	5.2	3.0	2.2
VI	17/10/2013	5	5.0	3.1	1.8	1.9	1.1	0.9	687.8	359.6	328.2	5.6	4.2	1.4

(section 1) during the flow tide, and $M_{DIN,ebb,S1} = 297$ g flowed out during the ebb tide, resulting in a net release of nitrogen ($\Delta M_{DIN,S1} = -149$ g) from the salt marsh to adjacent shallow waters (Fig. 4a, Table 1).

In contrast, during campaign II, $M_{DIN,flow,S1} = 461$ g flowed into the system and $M_{DIN,ebb,S1} = 279$ g flowed out into the salt marsh, resulting in a net sequestration of DIN ($\Delta M_{DIN,S1} = 182$; 39% $M_{DIN,flow,S1}$). Large amounts of nitrogen sequestration by the salt marsh were also observed in campaigns V and VI ($\Delta M_{DIN,S1} = +26$ g, +46% $M_{DIN,flow,S1}$ and $\Delta M_{DIN,S1} = +811$ g, +47% $M_{DIN,flow,S1}$).

The total suspended sediment (TSS) fluxes exhibited similar patterns. In campaign I, $M_{TSS,ebb,S1}$ (87 kg) was 5 times higher than $M_{TSS,flow,S1}$, indicating a net sediment export ($\Delta M_{TSS,S1} = -72.9$ kg). Vice versa, net sediment deposition (+20.7 kg) was revealed in campaign II ($M_{TSS,flow,S1} = 28$; $M_{TSS,ebb,S1} = 7$). Large sedimentation within the salt marsh was also observed in campaign V ($\Delta M_{TSS,S1} = +14.7$ kg, 48% of $M_{TSS,flow,S1}$), whereas no other relevant export events emerged.

The particulate organic carbon (POC) exhibited dynamics similar to TSS, as the POC concentration was in general related to sediment resuspension and deposition. In contrast, the dissolved organic carbon (DOC) often exhibited the opposite trend in terms of mass balance than other monitored parameters. In campaigns I and IV, despite the general export dynamics, the salt marsh acted as a sink of DOC; in contrast, during campaign II and V, the salt marsh acted as a source of DOC, whereas a net positive balance (import) was measured for all other components (Table 1). The calculated total mass ($\Delta M_{DIN,S}$, $\Delta M_{DOC,S}$, $\Delta M_{POC,S}$, $\Delta M_{TSS,S}$) that flowed through each monitored cross section (S) during each campaign is reported in Table B.2.

3.3. Factors controlling fluxes

Our results highlight the variability of fluxes during tidal cycles. Some authors discussed variability in nutrient fluxes in relation to seasonal dynamics. Daly and Mathieson (1981) observed a significant seasonal trend of Ammonia-N, being exported in winter and imported during the rest of the year. The results of Poulin et al. (2009), regarding seasonal nutrient fluxes variability, demonstrated the occurrence of seaward NH_4 fluxes and landward $NO_2 + NO_3$ fluxes over the entire year, whereas seasonal patterns were found for silicate, which was imported during high-productivity periods (May and July) and exported to estuarine waters during low-productivity periods (November and March). Dame et al. (1986) observed no seasonal trends for dissolved nitrogen, even though peak rates of ammonium export were measured in summer.

Although the dataset collected in this study is too limited to investigate seasonal variability, this does not seem to be the main factor controlling the salt marsh nitrogen sink or source behavior, since DIN import and export were observed in different seasons (import for March, July, October and export for September, May, June) (Table 2). Conversely, the amount of nitrogen flowing into the salt marsh during flow tide appeared to have an important role in determining the sign of the total mass budget. Nitrogen accumulation within the salt marsh ($\Delta M_{DIN,S1} > 0$) prevailed when large amounts of DIN entered the salt marsh (Table 1, campaigns II and VI).

The sediment fluxes presented similar dynamics, with deposition processes dominant for high values of $M_{TSS,flow}$ (campaign II and V). Eq. (1) shows that high concentrations of suspended sediment are essential for importing large amounts of sediments. In microtidal lagoons, the TSS concentration is driven by wave resuspension in adjacent bays. This process is particularly effective at remobilizing sediments from shallow waters (Fagherazzi et al., 2013, 2007; Ganju et al., 2005, 2013; Carniello et al., 2005). Fagherazzi and Priestas (2010) observed that the best conditions for sediment accumulation within salt marshes are moderate storms, which increase sediment resuspension near salt marshes but do not trigger fast flows in the tidal channels. These conditions characterized campaigns II and V, which revealed large sediment accumulation within the study site ($\Delta M_{TSS,S1} = 20.7$ and +14.7 kg), confirming the role of the abovementioned controlling factors.

During most intense surge events, even if large amounts of sediment are provided to the salt marsh during flooding, high tidal currents support sediment resuspension from the creek bottom and banks (Fagherazzi et al., 2013) and can result in a net negative sediment balance. This was the case for campaign I, which was characterized by the most intense hydrodynamic forcing (Fig. 3a) and a low TSS concentration in the water flowing into the salt marsh during flooding (Table 2). This resulted in a large export of sediments from the salt marsh to the adjacent shallow waters ($\Delta M_{TSS,S2} = -72.9$ kg). The observed sediment export during intense surge events supports the findings of D'Alpaos et al. (2007), who described, based on field observations and morphodynamic modeling of the same experimental site, the rapid development of a small creek network. These authors also highlighted the presence of a bank erosion process within the larger creek, leading to smoothing of the cross-sectional geometry.

The role of concentrations in water entering the salt marsh and hydrodynamic forcing as factors controlling the flux dynamics, previously

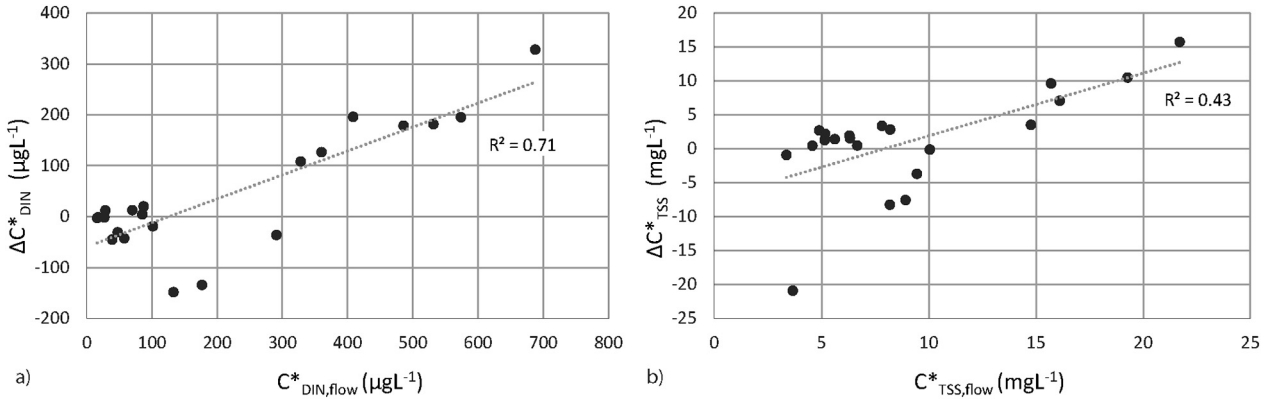

Fig. 5. Correlation between changes in C*between flow and ebb tides ($\Delta C^* = C^*_{flow} - C^*_{ebb}$) and inflow concentration C^*_{flow} for DIN (a) and TSS (b).

discussed from a qualitative perspective, was investigated in detail via statistical analysis.

The changes in the volume-weighted mean concentration (see Section 2.6, Eq. (4), Table 2), C^*_{DIN} and C^*_{TSS}, between flow and ebb tide ($\Delta C^*_S = C^*_{flow} - C^*_{ebb}$), were significantly correlated with the inflow concentration $C^*_{DIN,flow}$ ($r^2 = 0.71$, $p < 0.001$) and $C^*_{TSS,flow}$ ($r^2 = 0.4$, $p < 0.005$), respectively (Fig. 5). Similarly, ΔC^*_{DOC} and ΔC^*_{POC} were significantly correlated with $C^*_{DOC,flow}$ and $C^*_{POC,flow}$ ($r^2 = 0.30$, $p < 0.01$; $r^2 = 0.43$, $p < 0.005$).

The salt marsh acted as a sink of nitrogen and sediments when the concentrations flowing into the system were high. The positive correlation between $C^*_{DIN,flow}$ and ΔC^*_{DIN} is compatible with a first-order decay kinetic model for nutrient removal (Kadlec and Knight, 1996). A positive relation between inflow sediment concentration and deposition, here evaluated based on the initial $C^*_{TSS,flow,S}$ and $\Delta C^*_{TSS,S}$, was observed, as in the literature. In particular, Fagherazzi et al. (2013) and Reed et al. (1999) described the decrease in concentration and deposition rate along the flow path on the salt marsh with a simple first-order model, highlighting changes in deposition due to the distance from channel banks entering the marsh.

Despite these correlations, $C^*_{TSS,flow}$ per se does not correctly explain all changes in ΔC^*_{TSS}, in particular for campaign I, when the tidal excursion was higher than on the other sampling dates (Table B.1). Regarding the hypothesis that intense surges support sediment resuspension from the creek bottom and banks, contributing to net export of sediment away from the salt marshes, a Multiple Linear Regression (MLR) was performed. In the analysis, tidal excursion was used as a proxy for hydrodynamic forcing. As expected, the MLR equation showed that ΔC^*_{TSS} is positively correlated with $C^*_{TSS,flow}$ and negatively correlated with Δh_{tide} (MLR equation: $\Delta C^*_{TSS} = 0.77 + 0.91\ C^*_{TSS,flow} - 16.45\ \Delta h_{tide}$; multiple $r^2 = 0.60$; adjusted $r^2 = 0.55$; F-statistic = 11.32; $0.001 < p < 0.005$).

Despite the limited number of tidal cycles monitored, the six campaigns were representative of both normal and severe weather conditions. The frequency of tidal peaks higher than 0.68 m a.m.s.l. (as occurred on September 28th, 2011) is <8% (Venice Municipality – Tidal Forecasting Service; statistics based on hourly data collected from 1966 to 2016). High variability in the suspended sediment concentrations was observed, ranging from <5 mg L^{-1} (campaign I), typical of windless conditions, to 40 mg L^{-1} (campaign II). However, extreme events are not fully captured by this study. Indeed, during exceptionally high tides, which statistically occur once every 3 years, the water level rises above +1.15 m a.m.s.l. Moreover, under high Bora wind speed conditions, the TSS concentration is >100 mg L^{-1}. Therefore, future research could more deeply investigate the role of these extreme events using on-site continuous instruments for high-frequency monitoring (Etheridge et al., 2015; Ganju et al., 2005).

3.4. Functional roles of individual morphological elements

The monitoring design enabled an investigation of the distinctive processes occurring within each morphological element (creek 1, pond 1, creek 2 and pond 2) and assessment of their contribution to mass balance (see Sections 2.1, 2.2, Figs. 1, and 2). In particular, the total mass balance within each morphological element ($M_{DIN,E}$, $M_{TSS,E}$, $M_{DOC,E}$, $M_{POC,E}$) was calculated using Eq. (3) (Table 3).

This analysis highlighted the role of the intertidal vegetated area (pond 1) in nutrient removal processes. The vegetated pond acted as a sink of nitrogen in all campaigns except IV. Major nutrient removal occurred in campaign II (192 g) and VI (227 g). It is interesting to note that within this area, nitrogen sequestration processes prevailed over release also in campaign I ($\Delta M_{DIN,pond\_1} = 134$ g), during which the salt marsh overall acted as a DIN source (Table 1). These findings corroborate the results obtained by Piehler and Smyth (2011) regarding habitat-specific distinctions in estuarine denitrification. They highlighted significantly higher rates of denitrification in structured vegetated habitats than in intertidal and subtidal unvegetated flats. Only during campaign IV was a negative DIN balance observed within the vegetated pond ($\Delta M_{DIN,pond\_1} = -52.9$ g). This difference is likely due to a lower tidal peak (+0.34 m a.m.s.l., Table B.1). This tidal condition produces minor flooding on the vegetated area and a water discharge mostly flowing within the creek bed, in the segment delimited between station 2 (cross section 2) and station 3 (cross section 3).

The analysis of sedimentation-erosion patterns ($\Delta M_{TSS,E}$, Table 3) showed that erosion processes ($\Delta M_{TSS} < 0$) prevailed within creek_1, while deposition ($\Delta M_{TSS} > 0$) prevailed in the inner area of the salt marsh (creek_2 + pond_2).

The tests for correlations between the tidal peak height (h_{max}) and mass balance in each morphological element (ΔM_E), represented in Fig. 6, indicated a significant negative correlation ($r^2 =$

Table 3
Calculation of total mass balance within each morphological element ($M_{DIN,E}$, $M_{TSS,E}$, $M_{DOC,E}$, $M_{POC,E}$) using Eq. (3) (see Section 2.5, Fig. 2).

Morphological element	Campaign	Date	$\Delta M_{DIN,E}$ (g)	$\Delta M_{TSS,E}$ (kg)
Creek 1	I	28/09/2011	−207.3	−49.7
Pond 1 (vegetated)	I	28/09/2011	133.8	−31.8
Creek 2 + pond 2	I	28/09/2011	−75.0	8.6
Creek 1	II	09/03/2012	−83.5	8.3
Pond 1 (vegetated)	II	09/03/2012	191.6	11.8
Creek 2 + pond 2	II	09/03/2012	73.9	0.5
Creek 1	III	26/06/2012	−84.4	1.0
Pond 1 (vegetated)	III	26/06/2012	30.7	−1.1
Creek 2 + pond 2	III	26/06/2012	10.5	2.5
Creek 1	IV	08/05/2013	87.7	−1.5
Pond 1 (vegetated)	IV	08/05/2013	−52.9	1.1
Creek 2 + pond 2	IV	08/05/2013	−62.8	−0.1
Creek 1	V	23/07/2013	22.9	−6.7
Pond 1 (vegetated)	V	23/07/2013	3.7	17.2
Creek 2 + pond 2	V	23/07/2013	−1.0	4.3
Creek 1	VI	17/10/2013	91.4	−7.6
Pond 1 (vegetated)	VI	17/10/2013	227.3	1.5
Creek 2 + pond 2	VI	17/10/2013	493.3	5.6

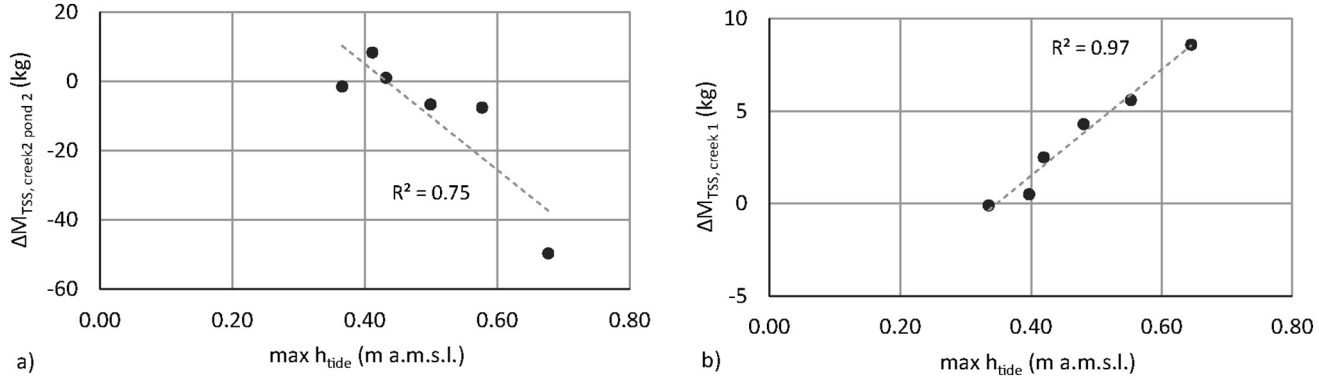

Fig. 6. Correlation between the highest tidal level reached during each campaign and the sediment mass budget within creek 1 (a) and within the inner area of the salt marsh (creek 2, pond 2) (b).

0.74, $p < 0.001$) for creek 1 and a positive correlation ($r^2 = 0.97$, $p < 0.001$) for creek 2. Following up on the discussion of the dual and opposite role of high-tide events in driving sediment dynamics within salt marshes (see Section 3.3), these correlations highlighted that during these events, the large amount of sediment entering the salt marsh supports sedimentation processes within the inner areas, whereas the higher resuspension capacity of tidal currents entails erosion in areas close to the creek mouth. These differences in sediment dynamics are explained by the higher intensity of hydrodynamic forcing in creek 1 than in creek 2, since tidal water fluxes are attenuated by bottom and bank friction during tide propagation (Fig. 2b).

Although more detailed studies are needed, these sedimentation-erosion patterns could explain the slope of the creek's bottom, growing from higher depth at cross section 1 (−0.40 m a.m.s.l.) to a depth at section 4 close to the mean sea level (+0.10 m a.m.s.l.).

4. Conclusion

Understanding the role that tidal salt marshes play in nutrient dynamics is still a critical issue in transitional water research. Studies regarding nutrient and organic matter tidal fluxes between salt marshes and adjacent waters receive significant attention from scientists and managers because of their influence on both water quality and the availability of essential elements at the base of the food web. Analyses of sediment fluxes are generally aimed at assessing the sedimentation dynamics within salt marshes and therefore their resilience potential to cope with sea level rises or alterations to sediment availability.

Most previous studies have discussed the tidal fluxes in ocean estuarine ecosystems, whereas little information about microtidal Mediterranean lagoons is available in the literature. In this study, a small microtidal reconstructed salt marsh was selected as the experimental site to investigate the sediment and nutrient fluxes and the factors controlling them. The specific features of this site (small dimensions and the water flux being forced to pass through a system of creeks and ponds without any possible lateral dispersion, therefore providing controllable and measurable boundary conditions) allowed further examination of the processes of sediment and nutrient accumulation and release over the tidal cycle.

The direction and magnitude of the fluxes between the salt marsh and adjacent waters were found to be highly variable. The studied salt marsh acted as a sink when high suspended solid and nutrient concentrations entered the salt marsh during flooding. Conversely, under a combination of low concentrations in the incoming water and high tidal excursion, the salt marsh works as a nutrient and sediment source. These dynamics suggest that salt marshes can operate as a water quality regulator, providing purification services by removing excess nutrients when concentrations are high and exporting nutrients to adjacent water, thereby supporting the primary production, when the concentrations in surrounding waters are low.

The analysis of the nutrient and sediment dynamics within the salt marsh highlighted the characteristic patterns of different morphological features. The nutrient removal function is provided by the intertidal vegetated area, which acted as a nitrogen sink of in all campaigns, even when the salt marsh overall exported a relatively large amount of nutrients.

Understanding the processes that regulate nutrient dynamics in salt marshes could support the design of restoration projects aimed at enhancing the provision of targeted ecosystem services. The results of this study suggest that (restored) salt marshes provide higher self-purification services in the presence of high nutrient concentrations and variability. Generally, in microtidal coastal lagoons, these conditions occur in inner landward areas, which are directly influenced by river inputs from the watershed and often characterized by intensive agriculture land use. In these areas, strengthening the self-purification functions could contribute to reducing the risk of eutrophication by acting as a filter when impulsive peaks of nutrient inputs occur. Moreover, large intertidal vegetated areas, revealed to be a major nutrient sink, should be taken into consideration when designing restorations to enhance water quality regulation services.

Moreover, ensuring the appropriate morphological functioning of salt marshes, with an appropriate design of creeks and intertidal platforms, is essential for the long-term resilience of constructed coastal salt marshes and therefore for the ecosystem services that they are expected to provide. The results showed that sediment release was a dominant process in the outermost creek, whereas sedimentation processes prevailed in the inner area of the salt marsh because of the attenuation of hydrodynamic forcing by bottom and bank friction during tidal propagation. These results signify that to store sediments even under severe weather events, an inner drainage network should be included in the design of constructed salt marsh projects.

Despite the limited number of tidal cycles monitored in this study, the six campaigns were representative of both normal and severe weather conditions. However, further analyses are required to strengthen these results; high-frequency monitoring, possibly through on-site continuous measurement instruments, could support the investigation of the role of extreme events and support long-term flux assessments.

Acknowledgments

This research was supported by the Agreement of 24/12/2008 of the Italian Ministry of the Environment and Protection of Land and Sea – Directorate General for the Environment, Land and Water Resources.

We would like to thank Andrea Pedroncini for support and valuable discussion about modeling, Federica Cacciatore for support during the statistical analysis, Federica Oselladore and Camilla Antonini for support during the field activities and Jane Da Mosto for revising the English. We would also like to thank the referees for their constructive comments and recommendations, which definitely helped to improve the quality of this paper.

Appendix A. Hydrodynamic numerical model setup, calibration and results

The hydrodynamic local conditions within the study-site were derived using the numerical model DHI-MIKE.

A flexible mesh was designed, combining triangular and rectangular elements (Fig. A.1 B, C), to properly describe the ponds topography and creeks bathymetry, respectively.

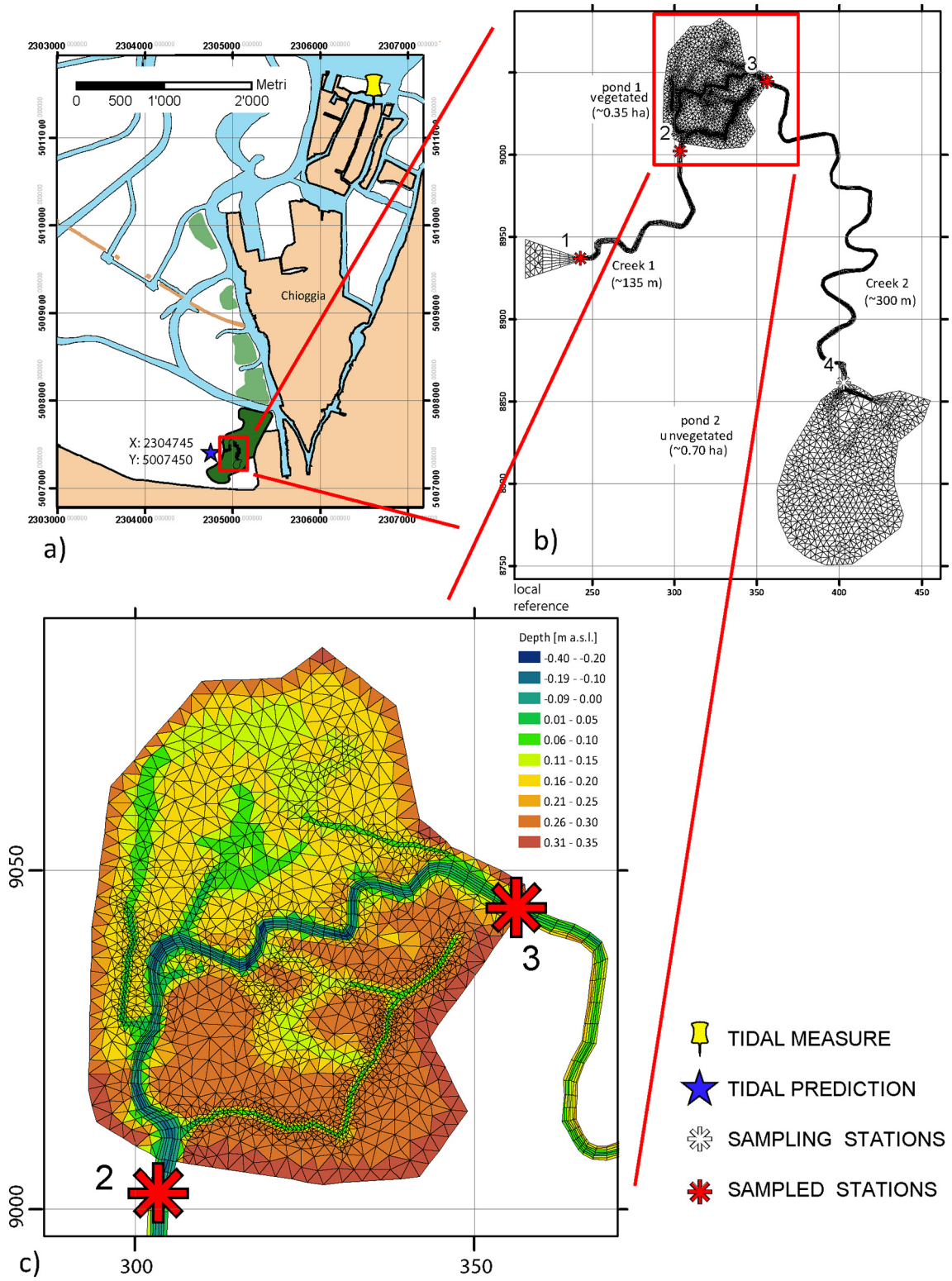

Fig. A.1. Model setup: A) position of measured and predicted tidal levels obtained by ISPRA within its activity in the Venice Lagoon (http://www.venezia.isprambiente.it/home) and used to force the DHI-Mike local model; B) DHI-Mike flexible mesh, with triangular and rectangular elements, to properly describe ponds surface and creeks; C) detail of the local mesh with the locations of sampling stations.

The model was forced using tidal and wind measures collected from a closed station (Chioggia-Vigo, Fig. A.1 A), which is part of the meteo-mareographic network of ISPRA. Additionally, the modeled levels, predicted daily by ISPRA for the entire Venice Lagoon, were considered to evaluate closer forcing conditions (http://www.venezia.isprambiente.it/home).

Measurements of the water level were collected during each campaign's tidal cycle at sampling stations to calibrate the hydrodynamic model (Fig. A.1 B, C).

In Fig. A.2, examples of the calibration results for stations 1 and 3 are presented. The roughness height parameter was varied between 1 cm to 20 cm, in relation to the vegetation (halophyte and submerged macrophytes) distribution in creek, salt marsh, and unvegetated pond. Finally, the best agreement between the simulation and observation was obtained for a homogeneous roughness height parameter of 5 cm.

The main differences between the observed and simulated water levels occurred in station 1 during the final phase of ebb flow, when the water level and discharge are truly small and do not have an influence on the total fluxes.

In Table A.1, calibration statistics are presented for the three stations.

In Fig. A.3, an example of the model results is presented. In particular, the total water depth distribution within the entire system is shown.

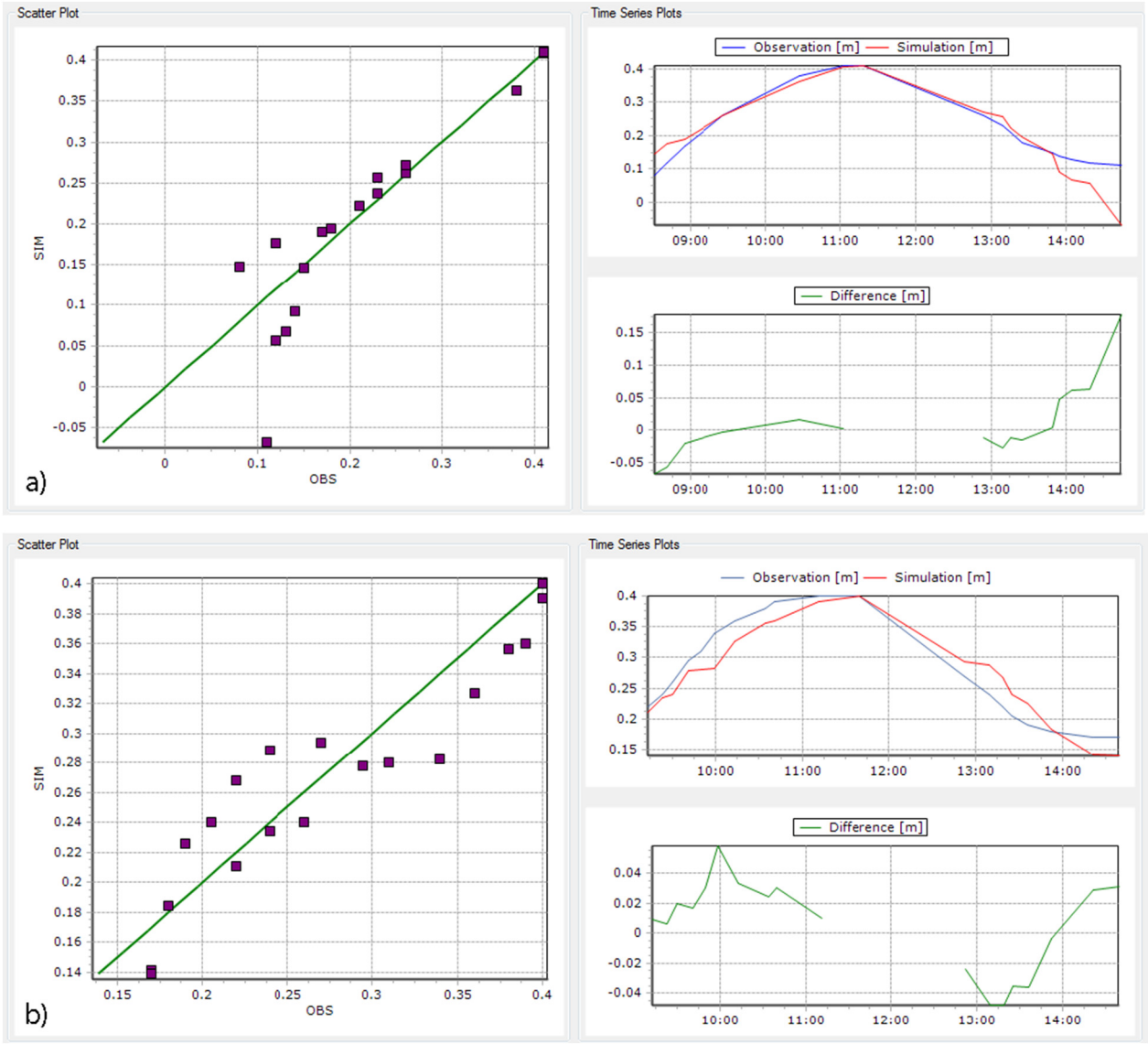

Fig. A.2. Example of calibration results for station 1 (a) and station 3 (b). Observed (OBS) and simulated (SIM) data are compared. The modeled data are obtained for a roughness height parameter of 5 cm.

Table A.1
Calibration statistics for stations 1, 2 and 3 obtained via comparison of observed and modeled results (DHI Time Series Comparison Tool).

		st.1	st.2	st.3
Mean error	[m]	0.01	−0.03	0.01
Mean absolute error	[m]	0.04	0.04	0.03
Root mean square error	[m]	0.06	0.05	0.03
Std. dev of residuals	[m]	0.05	0.04	0.03
Coefficient of determination	[−]	0.81	0.93	0.86
Coefficient of efficiency	[−]	0.80	0.62	0.83
Index of agreement	[−]	0.94	0.93	0.96

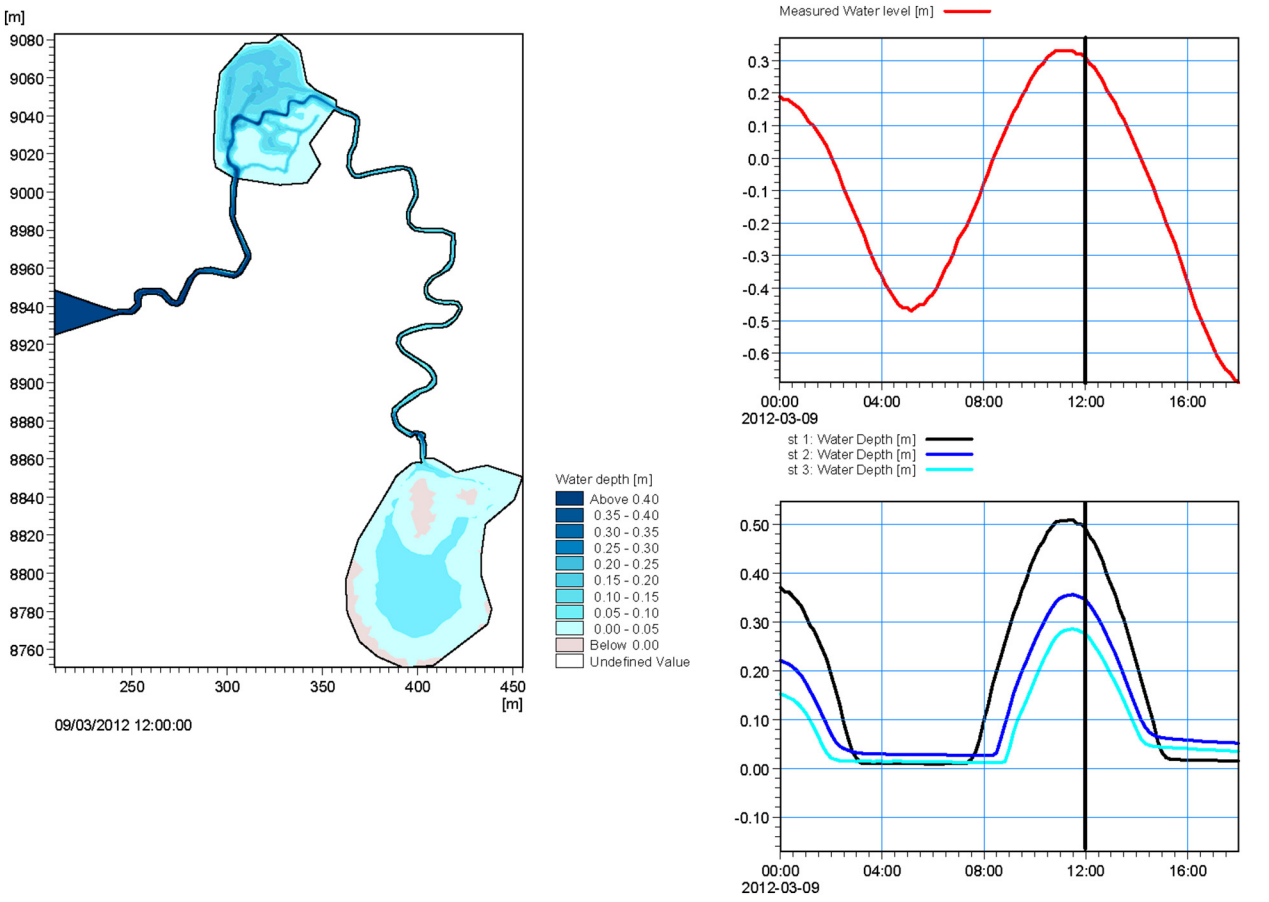

Fig. A.3. Model results for the 09/03/2012 campaign. Left: total water depth in the entire system; Top right: measured water level used as boundary condition to force the DHI-Mike model; Bottom right: modeled water level at different sampling stations (1-2-3).

Appendix B

Table B.1
Hydrodynamic parameters assessed by Mike-DHI HD Model at each cross section for all campaigns.

Campaign	Data	Cross section	Max h_{tide} (m a.m.s.l.)	Min h_{tide} (m a.m.s.l.)	Δh_{tide} (m)	Max Q_{flow} ($m^3\ s^{-1}$)	Max Q_{ebb} ($m^3\ s^{-1}$)	VOL_{flow} ($m^3 \times 10^3$)	VOL_{ebb} ($m^3 \times 10^3$)
I	28/09/2011	1	0.68	−0.13	0.81	0.38	−0.27	3.81	−3.53
I	28/09/2011	2	0.65	0.07	0.58	0.36	−0.25	3.59	−3.35
I	28/09/2011	3	0.65	0.12	0.52	0.25	−0.12	2.26	−2.05
II	09/03/2012	1	0.41	−0.20	0.61	0.14	−0.13	1.28	−1.19
II	09/03/2012	2	0.40	0.01	0.39	0.14	−0.10	1.18	−1.02
II	09/03/2012	3	0.40	0.07	0.33	0.07	−0.03	0.57	−0.52
III	26/06/2012	1	0.43	−0.09	0.53	0.15	−0.13	1.61	−1.53
III	26/06/2012	2	0.42	0.03	0.39	0.14	−0.10	1.51	−1.35
III	26/06/2012	3	0.42	0.07	0.35	0.08	−0.04	0.85	−0.77
IV	08/05/2013	1	0.37	0.12	0.25	0.17	−0.09	0.68	−0.80
IV	08/05/2013	2	0.34	0.11	0.22	0.15	−0.07	0.57	−0.68
IV	08/05/2013	3	0.34	0.12	0.22	0.05	−0.03	0.21	−0.32
IV	08/05/2013	4	0.30	0.24	0.06	0.03	−0.03	0.19	−0.28
V	23/07/2013	1	0.50	−0.03	0.53	0.23	−0.17	1.90	−1.76
V	23/07/2013	2	0.48	0.07	0.41	0.23	−0.15	1.83	−1.57
V	23/07/2013	3	0.48	0.12	0.36	0.12	−0.06	0.95	−0.87
V	23/07/2013	4	0.39	0.27	0.12	0.12	−0.05	0.86	−0.79
VI	17/10/2013	1	0.58	−0.16	0.73	0.28	−0.28	3.06	−2.49
VI	17/10/2013	2	0.56	0.08	0.47	0.27	−0.26	2.87	−2.30
VI	17/10/2013	3	0.55	0.14	0.41	0.19	−0.11	1.81	−1.26
VI	17/10/2013	4	0.48	0.31	0.17	0.18	−0.10	1.63	−1.11

Max h_{tide}: highest tidal level.
Min h_{tide}: lowest tidal level.
Δh_{tide}: tidal excursion.
Max Q_{flow}: maximum discharge during the flow phase.
Max Q_{ebb}: maximum discharge during the ebb phase.
VOL_{flow}: total water volume flowed through the section during the flow phase.
VOL_{ebb}: total water volume flowed through the section during the ebb phase.

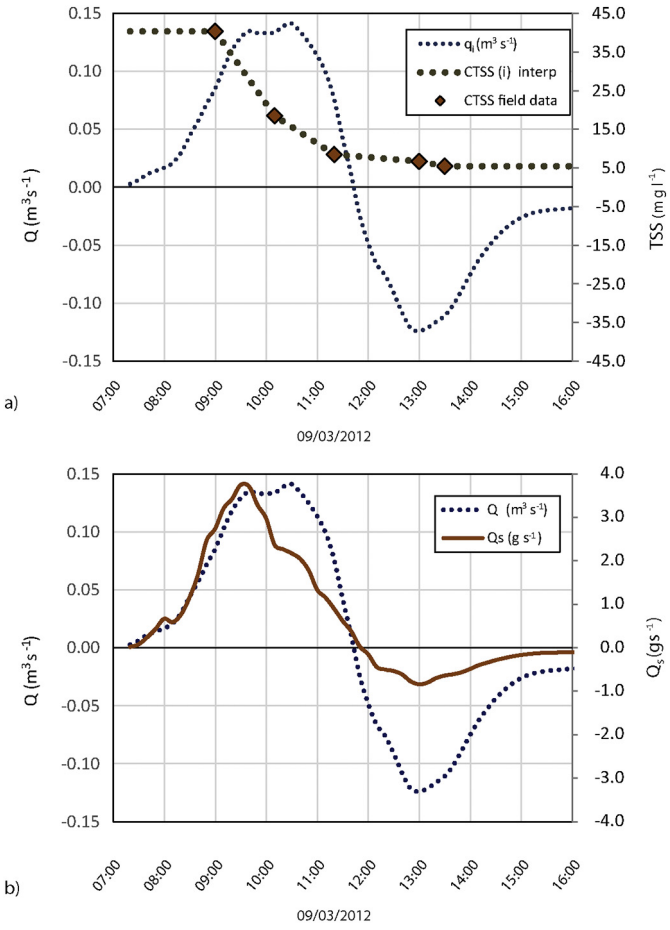

Fig. B.1. Example flux calculation based on field and interpolated data coupled with hydrodynamic modeling for the campaign on the 9th of March 2012. A) Measured and interpolated TSS concentrations (C_{TSS}) and water discharge q_i ($m^3\ s^{-1}$) at time step *i*. B) Sediment flow rate (Qs, $g\ s^{-1}$) calculated as $q_i c_i \Delta t$.

Table B.2
Calculated data of total mass flowed through each monitored cross section during each campaign. Positive values of ΔM (sink) are highlighted in blue, whereas negative values (source) are highlighted in red. Fluxes through section 1 are highlighted in bold.

Campaign	Data	Cross section	$M_{DIN,flow}$ (g)	$M_{DIN,ebb}$ (g)	ΔM_{DIN} (g)	$M_{TSS,flow}$ (kg)	$M_{TSS,ebb}$ (kg)	ΔM_{TSS} (kg)	$M_{DOC,flow}$ (kg)	$M_{DOC,ebb}$ (kg)	ΔM_{DOC} (kg)	$M_{POC,flow}$ (kg)	$M_{POC,ebb}$ (kg)	ΔM_{POC} (kg)
I	**28/09/2011**	**1**	**148**	**−297**	**−149**	**13.9**	**−86.8**	**−72.9**	**26.1**	**−18.0**	**8.1**	**2.3**	**−4.5**	**−2.3**
I	28/09/2011	2	251	−192	59	32.0	−55.2	−23.2	20.3	−21.3	−1.0	2.8	−3.5	−0.7
I	28/09/2011	3	130	−205	−75	17.7	−9.1	8.6	11.0	−13.0	−2.0	1.6	−1.5	0.0
II	**09/03/2012**	**1**	**461**	**−279**	**182**	**27.8**	**−7.1**	**20.7**	**3.1**	**−4.0**	**−0.9**	**0.7**	**−0.4**	**0.3**
II	09/03/2012	2	481	−216	266	18.5	−6.2	12.3	3.6	−3.5	0.1	0.6	−0.3	0.3
II	09/03/2012	3	187	−113	74	5.7	−5.2	0.5	1.6	−1.7	−0.1	0.2	−0.3	0.0
III	**26/06/2012**	**1**	**76**	**−120**	**−43**	**8.3**	**−5.9**	**2.3**	**7.1**	**−8.4**	**−1.3**	**1.2**	**−1.0**	**0.2**
III	26/06/2012	2	132	−90	41	6.9	−5.5	1.3	8.0	−8.6	−0.6	1.1	−0.5	0.7
III	26/06/2012	3	73	−62	10	4.2	−1.7	2.5	4.3	−4.1	0.1	0.6	−0.5	0.1
IV	**08/05/2013**	**1**	**69**	**−97**	**−28**	**4.5**	**−5.0**	**−0.5**	**6.6**	**−5.5**	**1.1**	**0.8**	**−0.9**	**−0.1**
IV	08/05/2013	2	76	−192	−116	4.7	−3.7	1.0	5.0	−5.0	0.0	0.8	−0.6	0.2
IV	08/05/2013	3	38	−101	−63	1.3	−1.4	−0.1	1.7	−2.7	−0.9	0.3	−0.3	−0.1
IV	08/05/2013	4	55	−93	−38	1.5	−4.7	−3.1	1.6	−2.8	−1.1	0.2	−1.1	−0.9
V	**23/07/2013**	**1**	**54**	**−29**	**26**	**30.6**	**−15.8**	**14.7**	**13.0**	**−13.7**	**−0.7**	**8.7**	**−6.6**	**2.0**
V	23/07/2013	2	32	−29	3	35.2	−13.7	21.4	13.2	−11.3	1.9	11.5	−5.1	6.5
V	23/07/2013	3	15	−16	−1	14.1	−9.8	4.3	7.6	−6.4	1.2	4.3	−3.6	0.7
V	23/07/2013	4	23	−22	1	8.1	−10.4	−2.3	8.0	−6.0	2.0	3.1	−3.5	−0.4
VI	**17/10/2013**	**1**	**1755**	**−943**	**812**	**10.3**	**−10.7**	**−0.4**	**9.8**	**−9.6**	**0.2**	**2.8**	**−2.4**	**0.3**
VI	17/10/2013	2	1526	−806	721	18.2	−11.0	7.2	10.8	−9.7	1.1	3.2	−2.2	1.0
VI	17/10/2013	3	879	−386	493	9.3	−3.7	5.6	7.8	−5.0	2.8	2.3	−1.1	1.2
VI	17/10/2013	4	1118	−399	719	9.1	−4.7	4.5	8.1	−3.5	4.6	3.2	−1.2	2.0

References

Carniello, L., Defina, A., Fagherazzi, S., D'Alpaos, L., 2005. A combined wind wave–tidal model for the Venice lagoon, Italy. J. Geophys. Res. 110 (F4), F04007. https://doi.org/10.1029/2004JF000232.

Costanza, R., d'Arge, R., de Groot, R., Farber, S., Grasso, M., Hannon, B., Naeem, S., Limburg, K., Paruelo, J., O'Neill, R.V., Raskin, R., Sutton, P., van den Belt, M., 1997. The value of the world's ecosystem services and natural capital. Nature 387, 253–260.

D'Alpaos, A., Lanzoni, S., Marani, M., Bonometto, A., Cecconi, G., Rinaldo, A., 2007. Spontaneous tidal network formation within a constructed salt-marsh: observations and morphodynamic modelling. Geomorphology 91, 186–197.

Daly, M.A., Mathieson, A.C., 1981. Nutrient fluxes within a small temperate salt marsh. Mar. Biol. 61, 337–344.

Dame, R.F., Chrzanowski, T., Bildstein, K., Kjerfve, B., McKellar, H., Nelson, D., Spurrier, J., Stancyk, S., Stevenson, H., Vernberg, J., Zingmark, R., 1986. The outwelling hypothesis and North Inlet, South Carolina. Mar. Ecol. Prog. Ser. 33, 217–229.

Erwin, K.L., 2009. Wetland and global climate change: the role of wetland restoration in a changing world. Wetl. Ecol. Manag. 17, 71–84.

Etheridge, J.R., Birgand, F., Osborne, J.A., Osburn, C.L., Burchell, M.R., Irving, J., 2014. Using in situ ultraviolet–visual spectroscopy to measure nitrogen, carbon, phosphorus, and suspended solids concentrations at a high frequency in a brackish tidal marsh. Limnol. Oceanogr. Methods 12, 10–22.

Etheridge, J.R., Birgand, F., Burchell II, M.R., 2015. Quantifying nutrient and suspended solids fluxes in a constructed tidal marsh following rainfall: the value of capturing the rapid changes in flow and concentrations. Ecol. Eng. https://doi.org/10.1016/j.ecoleng.2014.05.021.

Fagherazzi, S., Priestas, A.M., 2010. Sediments and water fluxes in a muddy coastline: interplay between waves and tidal channel hydrodynamics. Earth Surf. Process. Landf. 35 (3), 284–293.

Fagherazzi, S., Palermo, C., Rulli, M.C., Carniello, L., Defina, A., 2007. Wind waves in shallow microtidal basins and the dynamic equilibrium of tidal flats. J. Geophys. Res. 112, F02024. https://doi.org/10.1029/2006JF000572.

Fagherazzi, S., Wiberg, P.L., Temmerman, S., Struyf, E., Zhao, Y., Raymond, P.A., 2013. Fluxes of water, sediments, and biogeochemical compounds in salt marshes. Ecol. Process. 2, 1–16.

Ganju, N.K., Schoellhamer, D.H., Bergamaschi, B.A., 2005. Suspended sediment fluxes in a tidal wetland: measurement, controlling factors, and error analysis. Estuaries 28, 812–822.

Ganju, N.K., Nidzieko, N.J., Kirwan, M.L., 2013. Inferring tidal wetland stability from channel sediment fluxes: observations and a conceptual model. J. Geophys. Res. Earth Surf. 118, 1–14.

Ganju, N.K., Defne, Z., Kirwan, L.M., Fagherazzi, S., D'Alpaos, A., Carniello, L., 2017. Spatially integrative metrics reveal hidden vulnerability of microtidal salt marshes. Nat. Commun. 8, 14156.

Guarnieri, A., Vettore, A., Pirotti, F., Menenti, M., Marani, M., 2009. Retrieval of small-relief marsh morphology from terrestrial laser scanner, optimal spatial filtering, and laser return intensity. Geomorphology 113, 12–20.

Heinle, D.R., Flemer, D.A., 1976. Flows of material between poorly flooded tidal marshes and an estuary. Mar. Biol. 35, 359–373. https://doi.org/10.1007/BF00386646.

Kadlec, R.H., Knight, R.L., 1996. Treatment Wetlands. CRC Press, Boca Raton, FL (893 pp.).

Marani, M., Belluco, E., D'Alpaos, A., Defina, A., Lanzoni, S., Rinaldo, A., 2003. On the drainage density of tidal networks. Water Resour. Res. 39 (2), 1040. https://doi.org/10.1029/2001WR001051.

Mariotti, G., Fagherazzi, S., 2013. Critical width of tidal flats triggers marsh collapse in the absence of sea-level rise. Proc. Natl. Acad. Sci. U. S. A. 110, 5353–5356. https://doi.org/10.1073/pnas.1219600110.

Moharir, R.V., Khairnar, K., Paunikar, W.N., 2014. MIKE 3 as a modeling tool for flow characterization: a review of applications on water bodies. Int. J. Adv. Stud. Comput. Sci. Eng. 3 (3), 32–43.

Morris, J.T., Sundareshwar, P.V., Nietch, C.T., Kjerfve, B., Cahoon, D.R., 2002. Responses of coastal wetlands to rising sea level. Ecology 83, 2869–2877.

Mossman, H.L., Davy, A.J., Grant, A., 2012. Does managed coastal realignment create saltmarshes with 'equivalent biological characteristics' to natural reference sites? J. Appl. Ecol. 49, 1446–1456.

Mudd, S.M., Howell, S.M., Morris, J.T., 2009. Impact of dynamic feedbacks between sedimentation, sea-level rise, and biomass production on near surface marsh stratigraphy and carbon accumulation. Estuar. Coast. Shelf Sci. 82 (3), 377–389.

Odum, E.P., 1980. The status of three ecosystem-level hypotheses regarding salt marsh estuaries: tidal subsidy, outwelling and detritus-based food chains. In: Kennedy, V. (Ed.), Estuarine Perspectives. Academic Press, New York, pp. 485–495.

Piehler, M.F., Smyth, A.R., 2011. Habitat-specific distinctions in estuarine denitrification affect both ecosystem function and services. Ecosphere 2, 1–16.

Poulin, P., Pelletier, E., Koutitonski, C.G., Neumeier, U., 2009. Seasonal nutrient fluxes variability of northern salt marshes: examples from the lower St. Lawrence Estuary. Wetl. Ecol. Manag. 17, 655–673.

R Development Core Team. R, 2005. A Language and Environment for Statistical Computing. R Foundation for Statistical Computing, Vienna, Austria. http://www.R-project.org.

Reed, D.J., 1989. Patterns of sediment deposition in subsiding salt marshes, Terrebonne Bay, Louisiana: the role of winter storms. Estuaries 12 (4), 222–227.

Reed, D.J., Spencer, T., Murray, A.L., French, J.R., Leonard, L., 1999. Marsh surface sediment deposition and the role of tidal creeks: implications for created and managed coastal marshes. J. Coast. Conserv. 5, 81–90.

Rosencranz, J., Ganju, N., Ambrose, R., Brosnahan, S., Dickhudt, P., Guntenspergen, G., MacDonald, G., Takekawa, J., Thorne, K., 2016. Balanced sediment fluxes in southern California's Mediterranean-climate zone salt marshes. Estuar. Coasts 39, 1035–1049.

Sfriso, A., Facca, C., Bonometto, A., Boscolo, R., 2014. Compliance of the Macrophyte Quality index (MaQI) with the WFD (2000/60/EC) and ecological status assessment in transitional areas: the Venice lagoon as study case. Ecol. Indic. 46, 536–547.

Simas, T.C., Ferreira, J.G., 2007. Nutrient enrichment and the role of salt marshes in the Tagus estuary (Portugal). Estuar. Coast. Shelf Sci. 75, 393–407.

Strickland, J.D.H., Parsons, T.R., 1972. A practical handbook of seawater analysis. Bulletin of the Fisheries Research Board of Canada 167, 311.

Temmerman, S., Meire, P., Bouma, T.J., Herman, P.M., Ysebaert, T., De Vriend, H.J., 2013. Ecosystem-based coastal defence in the face of global change. Nature 504 (7478), 79–83. https://doi.org/10.1038/nature12859.

Velinsky, D.J., Paudel, B., Belton, T.J., Sommerfield, C.K., 2017. Tidal marsh record of nutrient loadings in Barnegat Bay, New Jersey. In: Buchanan, G., Belton, T.J., Paudel, B. (Eds.), A Comprehensive Assessment of Barnegat Bay–Little Egg Harbor, New Jersey. Journal of Coastal Research vol. 78, pp. 79–88.

Whiting, Gary J., McKellar Jr., Henry N., Kjerfve, Bjorn, Spurrier, John D., 1985. Sampling and computational design of nutrient flux from a southeastern U.S. saltmarsh. Estuar. Coast. Shelf Sci. 21 (2), 273–286.